



TpiA is a Key Metabolic Enzyme That Affects Virulence and Resistance to Aminoglycoside Antibiotics through CrcZ in *Pseudomonas aeruginosa*

Yushan Xia,^a Dan Wang,^a Xiaolei Pan,^a Bin Xia,^a Yuding Weng,^a Yuqing Long,^a Huan Ren,^a Jingyi Zhou,^a Yongxin Jin,^a Fang Bai,^a Zhihui Cheng,^a Shouguang Jin,^b Weihui Wu^a

^aState Key Laboratory of Medicinal Chemical Biology, Key Laboratory of Molecular Microbiology and Technology of the Ministry of Education, Department of Microbiology, College of Life Sciences, Nankai University, Tianjin, China

^bDepartment of Molecular Genetics and Microbiology, College of Medicine, University of Florida, Gainesville, Florida, USA

ABSTRACT Carbon metabolism plays an essential role in bacterial pathogenesis and susceptibility to antibiotics. In *Pseudomonas aeruginosa*, Crc, Hfq, and a small RNA, CrcZ, are central regulators of carbon metabolism. By screening mutants of genes involved in carbon metabolism, we found that mutation of the *tpiA* gene reduces the expression of the type III secretion system (T3SS) and bacterial resistance to aminoglycoside antibiotics. TpiA is a triosephosphate isomerase that reversibly converts glyceraldehyde 3-phosphate to dihydroxyacetone phosphate, a key step connecting glucose metabolism with glycerol and phospholipid metabolisms. We found that mutation of the *tpiA* gene enhances the bacterial carbon metabolism, respiration, and oxidative phosphorylation, which increases the membrane potential and promotes the uptake of aminoglycoside antibiotics. Further studies revealed that the level of CrcZ is increased in the *tpiA* mutant due to enhanced stability. Mutation of the *crcZ* gene in the *tpiA* mutant background restored the expression of the T3SS genes and the bacterial resistance to aminoglycoside antibiotics. Overall, this study reveals an essential role of TpiA in the metabolism, virulence, and antibiotic resistance in *P. aeruginosa*.

IMPORTANCE The increase in bacterial resistance against antibiotics imposes a severe threat to public health. It is urgent to identify new drug targets and develop novel antimicrobials. Metabolic homeostasis of bacteria plays an essential role in their virulence and resistance to antibiotics. Recent studies demonstrated that antibiotic efficacies can be improved by modulating the bacterial metabolism. *Pseudomonas aeruginosa* is an important opportunistic human pathogen that causes various infections. The bacterium is intrinsically resistant to antibiotics. In this study, we provide clear evidence that TpiA (triosephosphate isomerase) plays an essential role in the metabolism of *P. aeruginosa* and influences bacterial virulence and antibiotic resistance. The significance of this work is in identifying a key enzyme in the metabolic network, which will provide clues as to the development of novel treatment strategies against infections caused by *P. aeruginosa*.

KEYWORDS *Pseudomonas aeruginosa*, antibiotic resistance, carbon catabolite repression, triosephosphate isomerase, virulence

Pseudomonas aeruginosa is a ubiquitous opportunistic pathogen that causes a wide range of infections in humans, particularly in burn, immunodeficiency, and cystic fibrosis patients (1). *P. aeruginosa* harbors an arsenal of virulence factors that enable it to cause acute and chronic infections. The type III secretion system (T3SS) is a syringe-like machinery that directly injects effector proteins into host cells, leading to an

Citation Xia Y, Wang D, Pan X, Xia B, Weng Y, Long Y, Ren H, Zhou J, Jin Y, Bai F, Cheng Z, Jin S, Wu W. 2020. TpiA is a key metabolic enzyme that affects virulence and resistance to aminoglycoside antibiotics through CrcZ in *Pseudomonas aeruginosa*. mBio 11:e02079-19. <https://doi.org/10.1128/mBio.02079-19>.

Invited Editor Thomas Guillard, Inserm UMR-S P3Cell and CHU Reims

Editor Gerald B. Pier, Harvard Medical School

Copyright © 2020 Xia et al. This is an open-access article distributed under the terms of the [Creative Commons Attribution 4.0 International license](https://creativecommons.org/licenses/by/4.0/).

Address correspondence to Weihui Wu, wuweihui@nankai.edu.cn.

Received 1 October 2019

Accepted 21 November 2019

Published 7 January 2020

alteration of cellular function or cell death (2). The T3SS plays an essential role in acute infections caused by *P. aeruginosa* (3). Chronic infections caused by *P. aeruginosa* are usually accompanied by biofilm formation, in which the bacteria are protected from host immune cells and antimicrobial substances by the extracellular matrix (4, 5). Besides biofilm formation, a variety of mechanisms harbored by *P. aeruginosa* contribute to its antibiotic resistance, including antibiotic modification/hydrolysis enzymes, low membrane permeability, and multidrug efflux systems (6, 7).

Successful colonization requires a bacterium to quickly adjust its metabolism to adapt to the *in vivo* host environment. *P. aeruginosa* possesses complex metabolic pathways enabling it to utilize various carbon sources. Carbon catabolite repression (CCR) optimizes the bacterial metabolism and improves its ability to thrive in natural habitats (8). Hfq, Crc, and a small RNA, CrcZ, play pivotal roles in CCR in *P. aeruginosa*. Crc forms a complex with Hfq, which directly represses translation by binding to target mRNAs (9). In the presence of less-preferred carbon sources, a CbrA/CbrB two-component system activates the transcription of CrcZ (10, 11). CrcZ then binds to and sequesters Hfq, which in turn abrogates Hfq-mediated translational repression (12). Besides regulating metabolic genes, CCR also controls bacterial virulence and antibiotic resistance. For instance, a mutation of *crc* reduces the expression of *exsA*, the central regulator of the T3SS (13). The quorum sensing (QS) signal molecule synthetase RhlI is a target of the Lon protease. Crc represses the translation of *lon*, thus stabilizing the RhlI and promoting the *rhl* QS pathway (14). Hfq has also been shown to regulate biofilm formation and contribute to bacterial resistance to gentamicin, fosfomycin, and tetracycline (15, 16). Recent studies demonstrated that carbon sources and cellular respiration influence bacterial susceptibility to antibiotics (17, 18). Meylan et al. reported that fumarate increases bacterial cellular respiration and proton motive force (PMF) by stimulating the tricarboxylic acid (TCA) cycle in *P. aeruginosa*, which promotes the uptake of tobramycin. In contrast, glyoxylate decreases bacterial susceptibility to tobramycin by promoting the glyoxylate shunt, which represses cellular respiration (19). Therefore, perturbation of the metabolic network influences bacterial virulence and antibiotic resistance.

Here, we examined the cytotoxicity and antibiotic resistance of *P. aeruginosa* strains with mutations in the carbon metabolism genes. We found that mutation of the triosephosphate isomerase gene *tpiA* reduced the bacterial virulence and resistance to aminoglycoside antibiotics. Further studies revealed a critical regulatory role of CrcZ in the *tpiA* mutant.

RESULTS

Identification of carbon metabolic genes that affect bacterial cytotoxicity and antibiotic resistance. To understand the influences of carbon metabolic genes on the virulence and antibiotic resistance of *P. aeruginosa*, we screened all of the available mutants from the PA14 transposon insertion mutant library (20), including genes involved in the TCA cycle, glycolysis, and gluconeogenesis (Fig. 1A). Among the 40 tested strains, mutations in the *aceE*, *aceF*, *tpiA*, and *gpsA* genes displayed reduced cytotoxicity toward the human alveolar epithelial cell A549, whereas the *gltA* and *PA2843* mutants displayed enhanced cytotoxicity (see Fig. S1 in the supplemental material). Meanwhile, mutants of *gltA*, *fumC1*, *pykF*, and *lpd3* were less susceptible to tobramycin, while the *zwf* and *tpiA* mutants were more susceptible to tobramycin (Table S1).

Among all of the mutants tested, the *tpiA* mutant displayed simultaneous reduction in bacterial cytotoxicity and increased susceptibility to tobramycin to the greatest extent. The *tpiA* gene encodes a triosephosphate isomerase that catalyzes the reversible conversion from glyceraldehyde-3-phosphate (G3P) to dihydroxyacetone phosphate (DHAP). In *P. aeruginosa*, glucose is metabolized through the Entner-Doudoroff (ED) pathway via 6-phosphogluconate (Gnt6P) that is then dehydrogenated and turned into pyruvate and G3P (21, 22). Since *P. aeruginosa* lacks phosphofructokinase, it cannot transform fructose-6-phosphate into fructose-1,6-

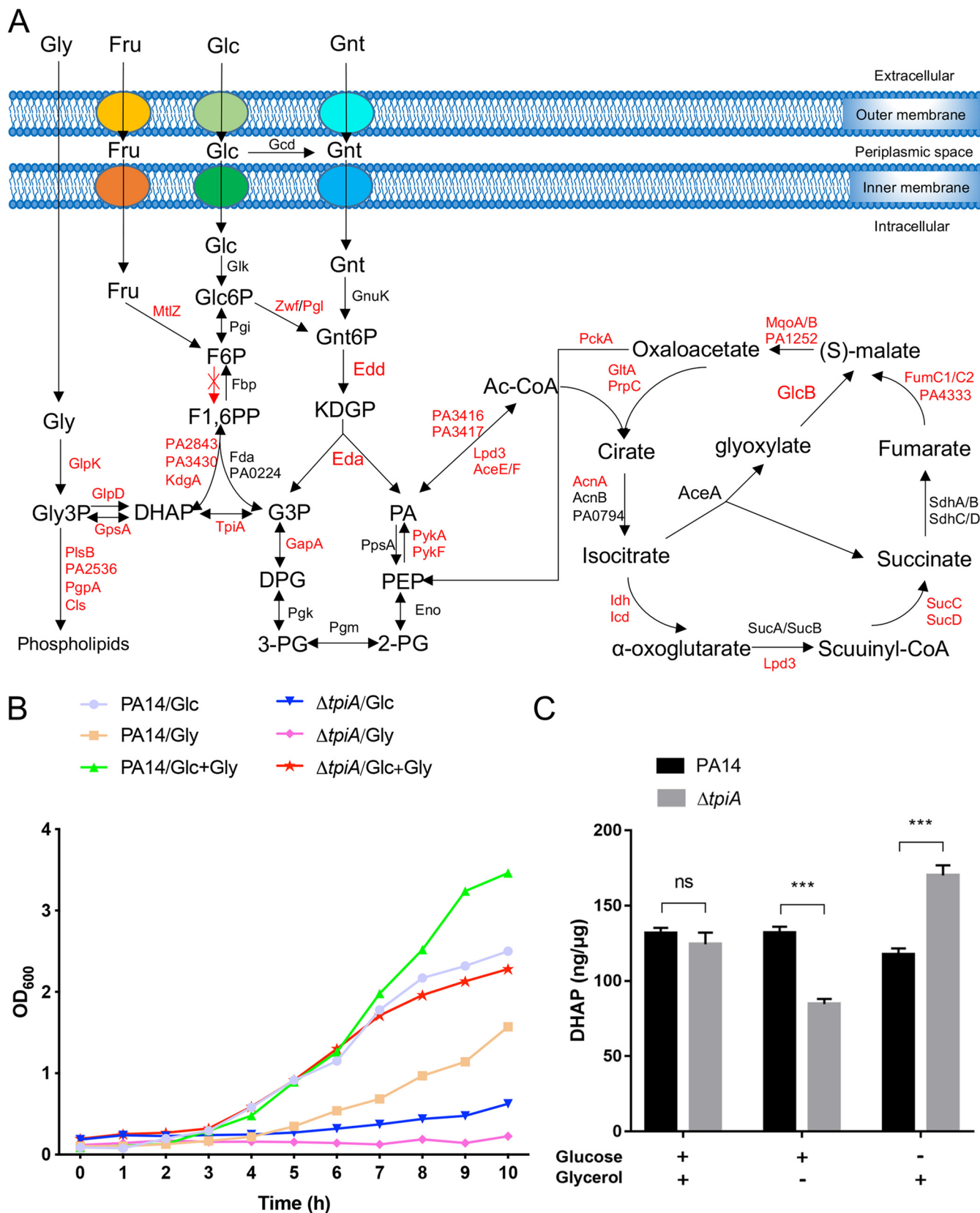


FIG 1 TpiA serves as a critical interlink between glycolysis and glycerol metabolism and phospholipid synthesis. (A) The glycolysis and tricarboxylic acid (TCA) cycle in *P. aeruginosa*. Most *Pseudomonas* species lack the phosphofruktokinase that transforms fructose-6-phosphate (F6P) into fructose-1,6-biphosphate (F1,6PP) (highlighted with a crossed-out red arrow). Therefore, G3P and DHAP are not directly derived from glucose through the classical Embden-Meyerhof- (Continued on next page)

biphosphate. Thus, the TpiA-mediated conversion between G3P and DHAP serves as a critical link between glycolysis/gluconeogenesis and glycerol metabolism/phospholipid synthesis (23). Indeed, a severe growth defect was observed when a $\Delta tpiA$ mutant was cultured in a M9 medium with glucose or glycerol as the sole carbon source. When glycerol was the sole carbon source, the $\Delta tpiA$ mutant displayed no obvious growth after 10 h. When glucose was the sole carbon source, the maximum growth rates (MGR) of the $\Delta tpiA$ mutant and the wild-type PA14 were 0.03/h and 0.29/h, respectively (Fig. 1B). However, simultaneous supplementation of both glucose and glycerol enabled the growth of the $\Delta tpiA$ mutant (Fig. 1B), resulting in the similar MGR in the $\Delta tpiA$ mutant and the wild-type PA14 (0.33/h and 0.32/h, respectively).

To further verify the function of TpiA, wild-type PA14 and the $\Delta tpiA$ mutant were grown in M9 medium with both glucose and glycerol as the carbon sources to an optical density at 600 nm (OD_{600}) of 1.0, which resulted in similar intracellular concentrations of DHAP in the two strains (Fig. 1C). However, the intracellular concentration of DHAP was lower in the $\Delta tpiA$ mutant 1 h after the bacteria were switched into the medium with glucose as the sole carbon source, and the reverse was the case when glycerol was the sole carbon source (Fig. 1C). In combination, these results demonstrated a critical role of TpiA in the carbon metabolism of *P. aeruginosa*.

The type III secretion system is defective in the *tpiA* mutant. Similar to the *tpiA::Tn* mutant, the $\Delta tpiA$ mutant displayed defective cytotoxicity, which was restored by complementation with the *tpiA* gene (Fig. 2A). Since the T3SS plays a critical role in the cytotoxicity of *P. aeruginosa*, we examined the expression levels of several T3SS genes, including the regulatory genes *exsA*, *exsC*, and *exsD*, the needle tip component gene *pcrV*, and the effector gene *exoU*. The *tpiA* mutant showed reduced expression of all of those genes, which was restored by complementation with the *tpiA* gene (Fig. 2B). Overexpression of the T3SS master regulatory gene *exsA* restored the mRNA levels of the *exsC*, *exsD*, *pcrV*, and *exoU* genes and the cytotoxicity of the $\Delta tpiA$ mutant (Fig. 2C and D). These results suggested that TpiA affects the expression of the T3SS genes.

Mutation of the *tpiA* gene increases bacterial susceptibility to aminoglycoside antibiotics. We then tested the role of TpiA in the bacterial resistance to various classes of antibiotics, including aminoglycosides, fluoroquinolones, tetracycline, polymyxin B, and β -lactams. Mutation of the *tpiA* gene did not affect the bacterial resistance to ciprofloxacin, ofloxacin, tetracycline, or carbenicillin. However, the $\Delta tpiA$ mutant exhibited increased susceptibility to all aminoglycoside antibiotics, with an 8-fold decrease in the MICs of tobramycin and a 4-fold decrease in the MICs of gentamicin, streptomycin, neomycin, and amikacin. Also, the $\Delta tpiA$ mutant exhibited a 2-fold decrease in the MIC of polymyxin B. Complementation with the *tpiA* gene restored the resistance to these antibiotics (Table 1). Since TpiA is involved in carbon metabolism, it may affect the bacterial antibiotic resistance differently in different nutrient environments. Therefore, we determined the MICs of aminoglycoside antibiotics in an artificial sputum medium (ASM) that had been used to mimic the lung environment of cystic fibrosis patients (24, 25). The $\Delta tpiA$ mutant displayed a 4-fold decrease in the MICs of gentamicin, neomycin, and amikacin and 8-fold decreases in the MICs of tobramycin and streptomycin (Table 2).

FIG 1 Legend (Continued)

Parnas (EMP) pathway, but rather from the ED pathway. The proteins labeled in red indicate that mutants of the corresponding genes were tested for cytotoxicity and antibiotic resistance. Glc, glucose; Gnt, gluconate; Fru, fructose; Glc6P, glucose-6-phosphate; Gnt6P, 6-phosphogluconate; KDPG, 2-keto-3-deoxy-6-phosphogluconate; G3P, glyceraldehyde-3-phosphate; DPG, 1,3-diphosphoglycerate; 3-PG, 3-phosphoglycerate; 2-PG, 2-phosphoglycerate; PEP, phosphoenolpyruvate; PA, pyruvate; DHAP, dihydroacetone phosphate; Ac-CoA, acetyl-coenzyme A; Gly, glycerol; Gly3P, glycerol-3-phosphate. (B) PA14 and the $\Delta tpiA$ mutant were grown overnight in LB. The bacteria were washed with PBS, and the same amount of the bacteria was inoculated in M9 medium with 40 mM glucose or 80 mM glycerol as the sole carbon source or containing both of the carbon sources (20 mM glucose and 40 mM glycerol). Bacterial growth was monitored by measuring the OD_{600} every hour for 10 h. (C) Bacterial intracellular DHAP levels. PA14 and the $\Delta tpiA$ mutant were grown in M9 medium with both 20 mM glucose and 40 mM glycerol to an OD_{600} of 1 and then washed three times with PBS. The bacteria were resuspended in M9 with 40 mM glucose or 80 mM glycerol as the sole carbon source and cultured for 1 h. The intracellular concentrations of DHAP were determined by a high-sensitivity dihydroxyacetone phosphate assay kit. The total protein levels were used as the internal controls. Data represent the mean \pm standard deviation of the results from three samples. ns, not significant; ***, $P < 0.001$ by Student's *t* test.

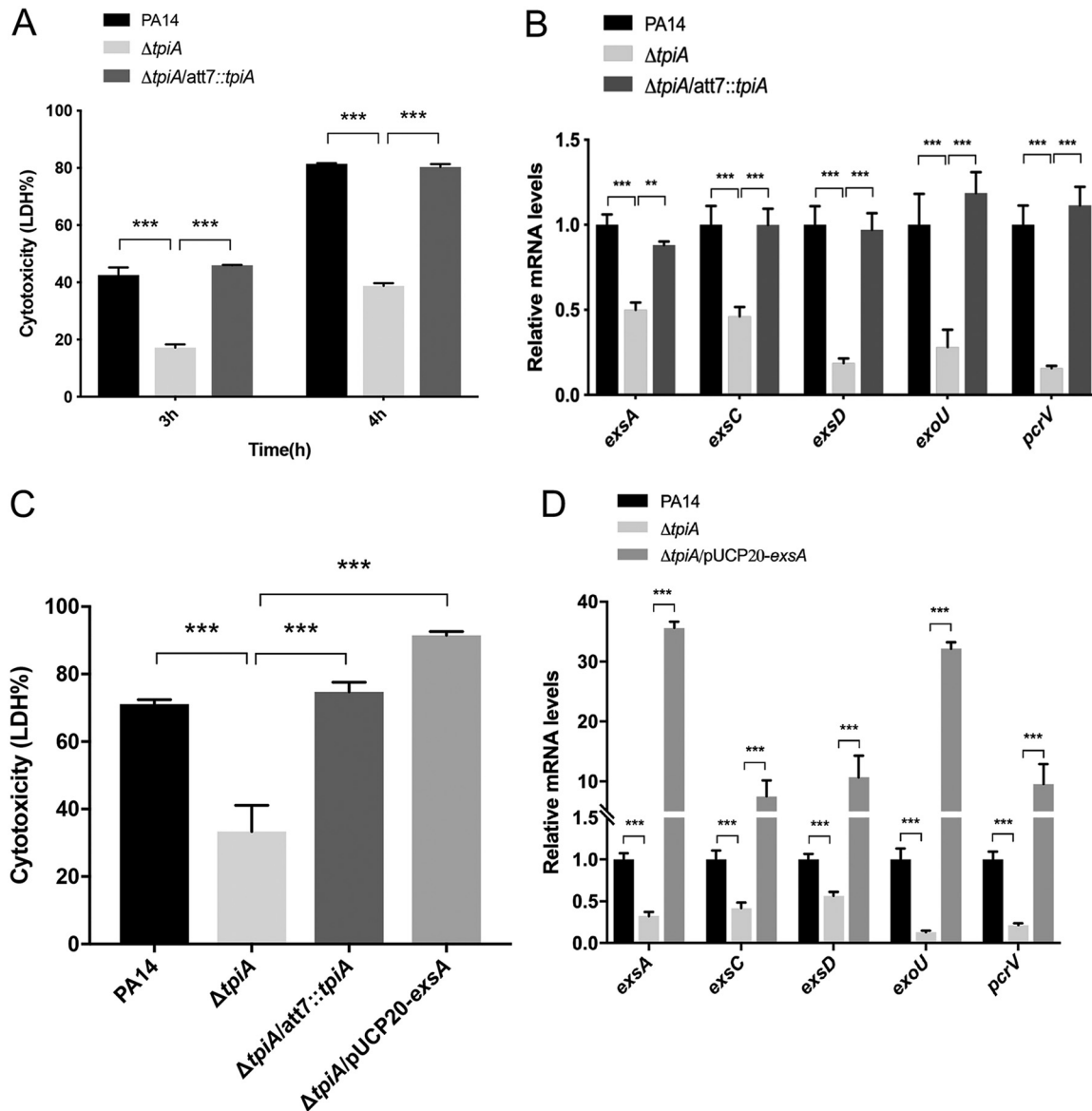


FIG 2 TpiA influences the T3SS. (A) Cytotoxicity of wild-type PA14, the $\Delta tpiA$ mutant, and the complemented strain. A549 cells were infected with the indicated strains at a multiplicity of infection (MOI) of 50 for 3 h or 4 h. The relative cytotoxicity was determined by the LDH release assay. (B) Wild-type PA14, the $\Delta tpiA$ mutant, and the complemented strain were grown in LB with 5 mM EGTA for 4 h. The relative mRNA levels of the T3SS genes were determined by real-time PCR. The 30S ribosomal protein gene *rpsL* was used as an internal control. (C) Cytotoxicity of the strains of wild-type PA14, the $\Delta tpiA$ mutant, the complemented strain, and the $\Delta tpiA$ mutant overexpressing *exsA*. A549 cells were infected with the bacteria with an MOI of 50 for 4 h. The relative cytotoxicity was determined by the LDH release assay. (D) The indicated bacterial strains were grown in LB with 5 mM EGTA for 4 h. The relative mRNA levels of the T3SS genes were determined by real-time PCR. The 30S ribosomal protein gene *rpsL* was used as an internal control. Data represent the mean \pm standard deviation of the results from three samples. *, $P < 0.05$; **, $P < 0.01$; ***, $P < 0.001$ by Student's *t* test.

Mutation of the *tpiA* gene increases the intracellular tobramycin level. Limiting intracellular drug levels is a major intrinsic resistance mechanism of *P. aeruginosa* against aminoglycoside antibiotics. Therefore, we measured tobramycin uptake by utilizing a Texas Red-labeled tobramycin (designated TbTR) (19). A larger amount of the TbTR was observed in the $\Delta tpiA$ mutant cells than in wild-type PA14 (Fig. 3A), whereas no difference was observed in the uptake of the free Texas Red (Fig. 3B). A previous study demonstrated that intracellular tobramycin activates the expression of genes involved in the heat shock response (26). Consistent with the TbTR uptake results, tobramycin treatment resulted in higher mRNA levels of the heat shock response genes, including *groES*, *ibpA*, and *hslV* in the $\Delta tpiA$ mutant, which were restored to the

TABLE 1 MICs of indicated strains in MHB

Strain	MIC ($\mu\text{g/ml}$) ^a										
	GEN	TOB	NEO	STR	AMK	TET	MEM	CAR	PMB	OFX	CIP
PA14	1	1	16	16	2	32	0.25	64	4	1	0.25
$\Delta tpiA$ mutant	0.25	0.125	4	4	0.5	32	0.25	64	2	1	0.25
$\Delta tpiA/att7::tpiA$	1	1	16	16	2	32	0.25	64	4	1	0.25

^aGEN, gentamicin; TOB, tobramycin; NEO, neomycin; STR, streptomycin; AMK, amikacin; TET, tetracycline; MEM, meropenem; CAR, carbenicillin; PMB, polymyxin B; OFX, ofloxacin; CIP, ciprofloxacin.

PA14 level by complementation with the *tpiA* gene (Fig. 3C). In combination, these results demonstrate increased tobramycin uptake by the $\Delta tpiA$ mutant.

The increased uptake of tobramycin is due to respiratory enhancement in the $\Delta tpiA$ mutant. The intracellular tobramycin level is largely influenced by efflux and uptake. The multidrug efflux system MexXY-OprM plays an important role in bacterial resistance to aminoglycoside antibiotics. Mutation or defective expression of *mexX* or *mexY* increases the bacterial susceptibility to aminoglycoside antibiotics (27, 28). Therefore, we examined whether mutation of *tpiA* affects the expression of *mexXY* in the presence or absence of tobramycin. The tobramycin was used at 0.1 mg/liter, at which no growth difference was observed between the wild-type PA14 and the $\Delta tpiA$ mutant (data not shown). The mRNA levels of *mexX*, *mexY*, and *oprM* were similar between wild-type PA14 and the $\Delta tpiA$ mutant in the presence or absence of tobramycin (Fig. S2).

We then examined whether TpiA influences the uptake of tobramycin. Previous studies revealed that the proton motive force (PMF) generated by the electron transport chain (ETC) is required for the uptake of tobramycin (Fig. 4A) (29). We used the dye 3,3'-diethylloxycarbocyanine iodide [$\text{DiOC}_2(3)$] to examine PMF-dependent membrane potential, which is represented by the ratio of red to green fluorescence (19, 30). As shown in Fig. 4B, mutation of *tpiA* enhanced the membrane potential. By utilizing an extracellular oxygen consumption assay kit and alamarBlue (31), we found that mutation of *tpiA* enhanced the bacterial ETC activity and respiratory rate (Fig. 4C and D). In addition, the levels of ATP and NADH were also increased in the $\Delta tpiA$ mutant (Fig. 4E and F).

To determine whether the enhanced respiratory activity is the cause of increased susceptibility to tobramycin in the $\Delta tpiA$ mutant, we treated the bacterial cells with Na_2ATP , an inhibitor of TCA cycle enzymes, including citrate synthase, isocitric dehydrogenase, and α -oxoglutarate dehydrogenase (32). In MHB, the $\Delta tpiA$ mutant grows slower than does the wild-type strain (Fig. S3A). Treatment with Na_2ATP reduced the growth rates of both of the strains (Fig. S3A). In addition, treatment with Na_2ATP reduced the membrane potential, intracellular NADH level, and uptake of tobramycin in both strains, diminishing the differences observed between the two strains without the Na_2ATP treatment (Fig. 5A to C). Furthermore, the presence of Na_2ATP increased the MICs of tobramycin for wild-type PA14 and the $\Delta tpiA$ mutant by 8- and 32-fold, respectively, which reduced the difference between the two strains from 8-fold to 2-fold (Table 3). Therefore, mutation of *tpiA* results in respiratory enhancement, which subsequently increases bacterial susceptibility to tobramycin.

Mutation of *tpiA* releases the carbon catabolite repression. Previous studies demonstrate that bacterial respiratory activity is closely related to the expression of the

TABLE 2 MICs of the aminoglycoside antibiotics to indicated strains in ASM

Strain	MIC ($\mu\text{g/ml}$) ^a				
	GEN	TOB	NEO	STR	AMK
PA14	2	2	64	16	4
$\Delta tpiA$ mutant	0.5	0.25	16	4	0.5

^aGEN, gentamicin; TOB, tobramycin; NEO, neomycin; STR, streptomycin; AMK, amikacin.

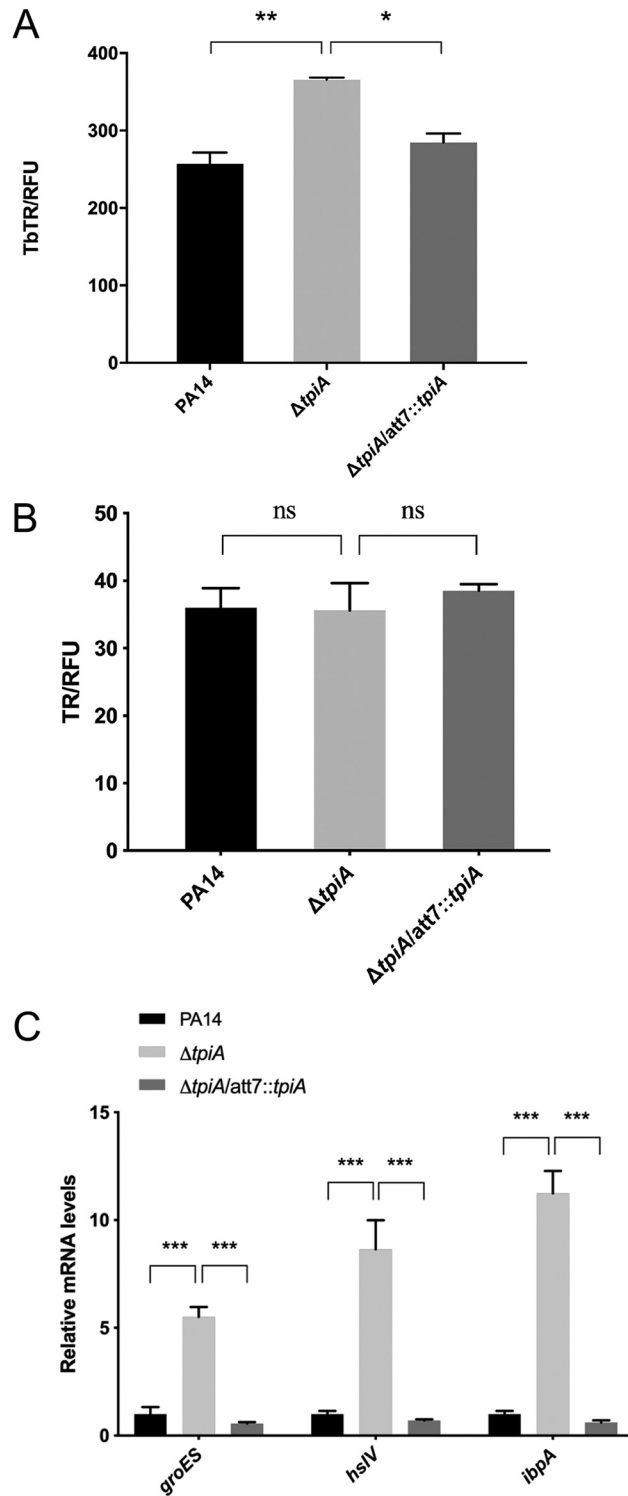


FIG 3 Mutation of *tpiA* increases the uptake of tobramycin. (A and B) Wild-type PA14, the $\Delta tpiA$ mutant, and the complemented strain were cultured in LB to an OD_{600} of 1, followed by incubation with 40 mg/liter tobramycin-Texas Red (TbTR) (A) or Texas Red (TR) (B) for 30 min. The bacteria were collected by centrifugation, washed three times with PBS, and then lysed in PBS by sonication. The Texas Red was excited at 595 nm, and the emission at 615 nm was measured with a luminometer. The relative fluorescence (measured in relative fluorescence units [RFU]) was normalized by the total protein amount. (C) The bacteria were treated with 0.1 mg/liter tobramycin for 30 min, followed by RNA isolation. The mRNA levels of *groES*, *hslV*, and *ibpA* were determined by real-time PCR. The 30S ribosomal protein gene *rpsL* was used as an internal control. Data represent the mean \pm standard deviation of the results from three samples. *, $P < 0.05$; **, $P < 0.01$; ***, $P < 0.001$; ns, not significant by Student's *t* test.

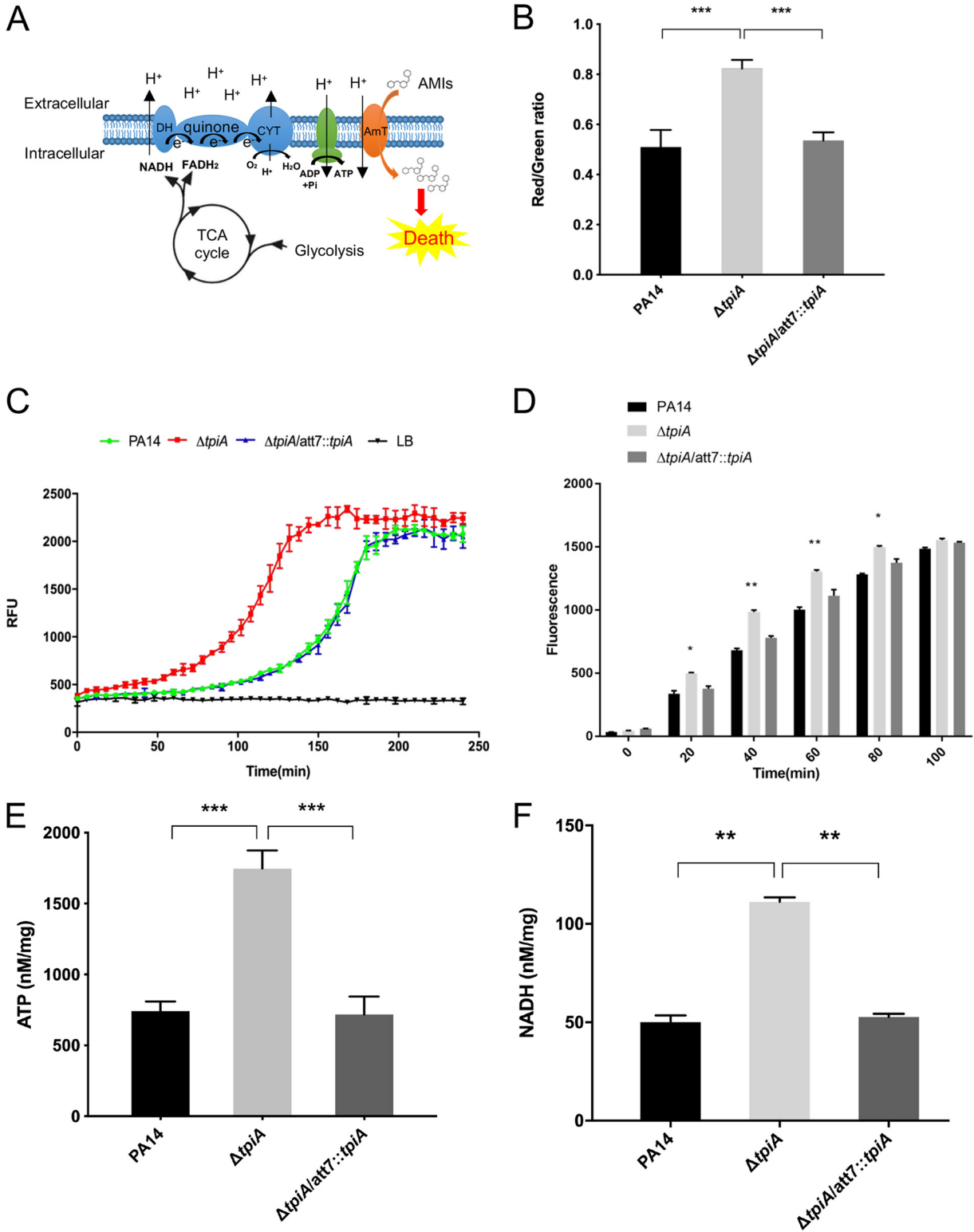


FIG 4 The increased uptake of tobramycin is due to respiratory enhancement in the *tpiA* mutant. (A) Schematic of the respiratory chain, glycolysis, and TCA cycle. DH, dehydrogenase; QE, quinone; CYT, cytochrome oxidase. Proton motive force (PMF) generated by the ETC drives aminoglycoside (19) uptake through a putative transporter (AmT). (B) Membrane potential was represented by the ratio of green to red fluorescence. The logarithmic-phase bacterial cells were incubated with DiOC₂(3) for 1 h and then subjected to flow cytometry analysis. Data represent the mean ± standard deviation of the results from three samples. ***, *P* < 0.001 by Student's *t* test. (C) Bacterial ETC activity. The ETC activities were quantified by an extracellular oxygen consumption assay kit. A total of 1.5 × 10⁵ bacterial cells in fresh LB were mixed with 10 μl of the O₂ consumption reagent in a black 96-well plate and sealed with 50 μl mineral oil to isolate the air. As the bacterial respire, oxygen is depleted in the surrounding environment, which is seen as an increase in phosphorescence signal. The fluorescence was measured every 5 min for 4 h. Data represent the

(Continued on next page)

ETC and central metabolic genes (19). To understand how TpiA affects bacterial respiration, we compared the transcriptomes of wild-type PA14 and the $\Delta tpiA$ mutant. A total 846 genes were differentially expressed in the $\Delta tpiA$ mutant. The GO and KEGG pathway enrichment analyses revealed that mutation of *tpiA* resulted in the upregulation of multiple carbon metabolism and ETC genes, including the aconitate hydratase gene *acnA*, fumarate hydratase gene *fumC2*, dihydrolipoamide dehydrogenase gene *lpd3* in the TCA cycle, the pyruvate dehydrogenase component subunit genes *PA3416* and *PA3417*, and the cytochrome *c* oxidase subunit genes *coxA*, *coxB*, *colIII*, *coiA*, and *PA4133* in oxidative phosphorylation (Fig. 6A and Table S2). In addition, multiple genes involved in amino acid and fatty acid metabolism were upregulated in the $\Delta tpiA$ mutant (Table S2). In *P. aeruginosa*, Crc, Hfq and a small RNA, CrcZ, play important roles in carbon catabolite repression (CCR) that globally regulates metabolic genes (9). The expression patterns of the above-described genes in the $\Delta tpiA$ mutant resemble those in a *crc* or *hfq* mutant (12, 33). We thus examined the expression levels of *crc*, *hfq*, and *crcZ* by real-time PCR. No significant change was observed in the expression of *crc* and *hfq*, whereas *crcZ* was upregulated in the $\Delta tpiA$ mutant (Fig. 6B), indicating a possible release of CCR. We then examined the translation efficiency of *amiE* (encoding the aliphatic amidase), which is inhibited by Crc and Hfq in CCR (11, 34). We constructed a translational fusion between a *lacZ* reporter gene and the CRC regulatory sequence of *amiE* (*amiE'*-*lacZ*) (11) as well as a C-terminal 6×His-tagged *amiE* (*amiE*-His), which are driven by an exogenous P_{tac} promoter and P_{BAD} promoter, respectively. The LacZ and *amiE*-His levels were higher in the $\Delta tpiA$ mutant than those in the wild-type PA14 and complemented strains (Fig. 6C and D), indicating a release of CCR.

Mutation of the *tpiA* gene increases the stability of CrcZ. To explore the mechanism of the CrcZ upregulation, we constructed a transcriptional fusion between the *lacZ* reporter gene and the promoter of *crcZ* (P_{crcZ} -*lacZ*). The LacZ levels were similar in wild-type PA14 and the $\Delta tpiA$ mutant (Fig. 7A). Consistently, no significant difference was observed in the known transcriptional regulatory genes of the *crcZ*, including *rpoN*, *cbrA*, and *cbrB* (Fig. 7B) (8). We then examined stability of CrcZ. After blockage of RNA transcription by rifampin, the CrcZ level dropped quickly in wild-type PA14, whereas a slower reduction was observed in the $\Delta tpiA$ mutant (Fig. 7C). Meanwhile, the rRNA RpsL level was reduced at a similar rate in the two strains (Fig. 7D). These results suggested that the higher level of CrcZ in the $\Delta tpiA$ mutant is likely due to its increased stability.

The increased CrcZ level in the $\Delta tpiA$ mutant contributes to its hypersusceptibility to aminoglycoside antibiotics. To examine the role of CrcZ in the $\Delta tpiA$ mutant, we knocked out *crcZ* in the PA14 and $\Delta tpiA$ mutant backgrounds. The deletion of *crcZ* in the $\Delta tpiA$ mutant partially restored the bacterial growth in MHB (Fig. S3B) but fully restored the intracellular ATP and NADH levels, respiratory activity, and membrane potential, as well as the uptake of tobramycin. However, no significant difference was observed between PA14 and its isogenic $\Delta crcZ$ mutant (Fig. 8A to E). Furthermore, deletion of *crcZ* in the $\Delta tpiA$ mutant restored the bacterial resistance to aminoglycoside antibiotics but did not affect the resistance in wild-type PA14 (Table 4). When treated with tobramycin, the expression levels of *groES*, *ibpA*, and *hslV* were increased in the $\Delta tpiA$ mutant but not in the PA14, $\Delta tpiA \Delta crcZ$ mutant, and $\Delta crcZ$ mutant strains (Fig. 8F).

FIG 4 Legend (Continued)

mean \pm standard deviation of the results from three samples. (D) Bacterial respiratory rates were quantified by alamarBlue, a nonfluorescent dye that emits pink fluorescence in the reduced state. A total of 2×10^8 bacterial cells in fresh LB were mixed with 20 μ l alamarBlue reaction solution in a black 96-well plate. The fluorescence was measured every 20 min for 2 h. Data represent the mean \pm standard deviation of the results from three samples. (E) Intracellular ATP levels were determined using an enhanced ATP assay kit. Bacteria were cultured in LB at 37°C to an OD₆₀₀ of 1. One and a half milliliters of the bacteria was collected and broken by ultrasound sonication in the lysis buffer. Measurement of the ATP level in the supernatant was performed according to the manufacturer's instruction. Total proteins were quantified by bicinchoninic acid (BCA) analysis for normalization. Data represents the mean \pm standard deviation from three samples. (F) Bacterial NADH levels were determined by an Amplitude fluorimetric NAD/NADH ratio assay kit. Bacteria were cultured in LB medium at 37°C to an OD₆₀₀ of 1. The bacteria were lysed in PBS buffer by sonication. Measurement of the NADH level in the supernatant was performed according to the manufacturer's instruction. Total proteins were quantified by BCA analysis for normalization. Data represent the mean \pm standard deviation of the results from three samples. **, $P < 0.01$; ***, $P < 0.001$ by Student's *t* test.

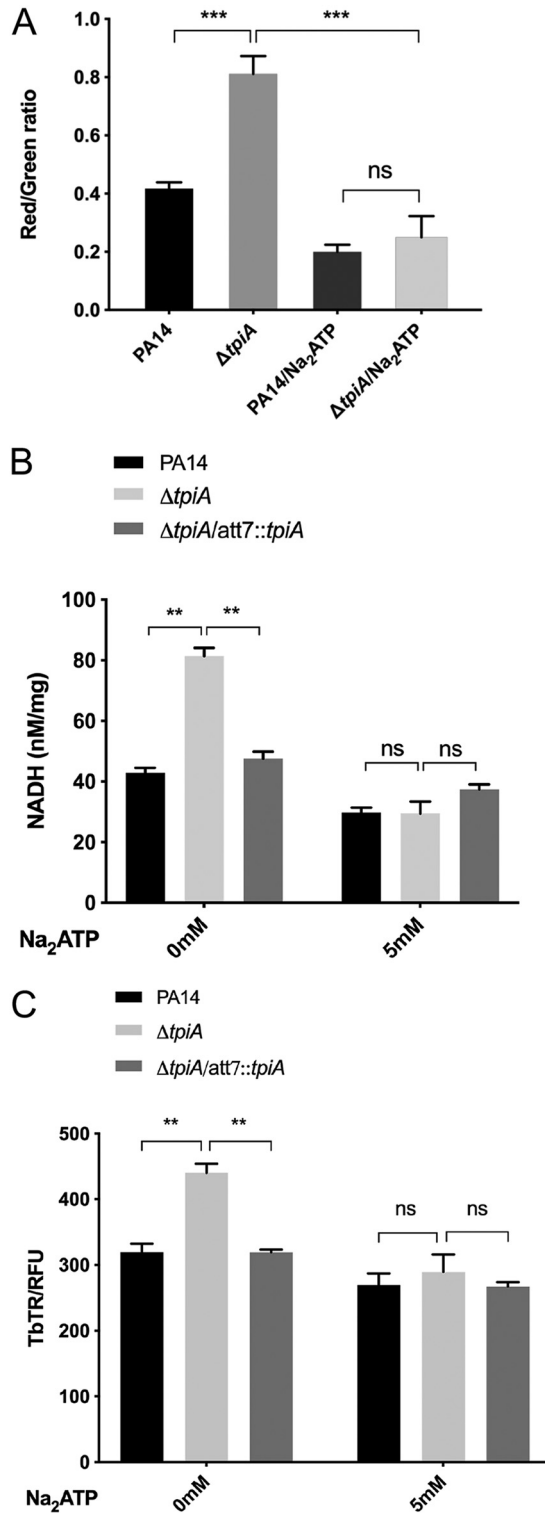


FIG 5 Inhibition of the TCA cycle restores the resistance of the $\Delta tpiA$ mutant to aminoglycoside antibiotics. (A) Effect of TCA inhibitor on membrane potential. PA14 and the $\Delta tpiA$ mutant were cultured in LB with or without 5 mM Na₂ATP to an OD₆₀₀ of 1. The bacteria were diluted to 10⁶ CFU/ml in PBS. Two microliters of 20 mM DiOC₃(3) was added to 1.5 ml of the bacterial suspension and incubated for 1 h at 37°C in dark, followed by flow cytometry analyses. (B) Effect of the TCA inhibitor on the NADH level. The bacteria were cultured in LB with or without 5 mM Na₂ATP to an OD₆₀₀ of 1. The bacterial cells were collected and lysed in PBS by sonication. Measurement of the NADH level in the supernatant was performed according to the manufacturer's instruction. (C) Effect of the TCA inhibitor on tobramycin uptake. The bacteria were cultured in LB with or without 5 mM Na₂ATP to an OD₆₀₀ of 1 and then

(Continued on next page)

TABLE 3 MICs of tobramycin against indicated strains in MHB with or without Na₂ATP

Strain	MIC ($\mu\text{g/ml}$)		
	0 mM	2 mM	5 mM
PA14	1	2	8
ΔtpiA mutant	0.125	1	4

CrcZ is involved in repression of the T3SS in the ΔtpiA mutant. It has been reported that Crc is required for the T3SS in *P. aeruginosa* (13). We thus hypothesized that the increased level of CrcZ might lead to repression of the T3SS in the ΔtpiA mutant. Indeed, expression of the T3SS genes and the cytotoxicity of the ΔtpiA mutant were restored by the deletion of *crcZ* (Fig. 9A and B). Since the T3SS plays an important role in acute infections of *P. aeruginosa*, we examined bacterial virulence in a murine acute pneumonia model. The deletion of *tpiA* attenuated bacterial virulence, which was restored by further deletion of the *crcZ* gene. Meanwhile, the deletion of *crcZ* in PA14 did not affect bacterial virulence (Fig. 9C). In LB, the growth rate of the ΔtpiA mutant was lower than that of the wild-type strain but was similar to those of the ΔcrcZ and $\Delta\text{crcZ } \Delta\text{tpiA}$ mutants. Overexpression of *exsA* in the ΔtpiA mutant ($\Delta\text{tpiA/pUCP20-exsA}$) further reduced the growth rate (Fig. S3C). However, the $\Delta\text{tpiA/pUCP20-exsA}$ mutant strain displayed the highest cytotoxicity, and the deletion of *crcZ* in the ΔtpiA mutant restored bacterial cytotoxicity and virulence in the murine acute pneumonia model. These results suggest that TpiA affects cytotoxicity and bacterial virulence mainly through CrcZ.

Since the *tpiA* mutant shows a growth defect, secondary mutations could occur to compensate the fitness defect. To further confirm that the phenotypes of the mutant strains are related to *tpiA* and *crcZ*, the strains used in this study have been subjected to whole-genome sequencing, including the wild-type PA14 and the three mutant strains, namely, the ΔtpiA , ΔcrcZ , and $\Delta\text{tpiA } \Delta\text{crcZ}$ mutants. In reference to the wild-type strain, the locations of the point mutations are shown in Fig. S4A and listed in Table S3. Frameshift mutations in the CTP synthetase gene *pyrG* were found in all three mutants. A previous study in *Mycobacterium tuberculosis* demonstrated that a mutation in *pyrG* actually increased bacterial resistance to various antibiotics, including aminoglycoside antibiotics (35). Three mutations were unique in the $\Delta\text{tpiA } \Delta\text{crcZ}$ mutant. The mutated genes are *glgB*, *thiC*, and *PA5393*, encoding a 1,4- α -glucan branching enzyme, a thiamine biosynthesis enzyme, and a hypothetical protein, respectively. Strains with a mutation in each of these genes were obtained from the PA14 transposon insertion mutant library (20). All three mutants displayed the same antibiotic resistance level to tobramycin (MIC, 1 $\mu\text{g/ml}$) and a similar level of cytotoxicity as those of the wild-type PA14. These results suggest that the decreased antibiotic resistance and cytotoxicity of the *tpiA* mutant are mainly due to the upregulation of CrcZ, ruling out the secondary mutational effect.

DISCUSSION

Here, we investigated the roles of carbon metabolism-related genes on virulence and aminoglycoside antibiotic susceptibility in *P. aeruginosa*. We found that mutation of the triosephosphate isomerase gene *tpiA* resulted in the most profound defect in bacterial virulence and antibiotic resistance against aminoglycoside antibiotics.

TpiA is a highly conserved enzyme that catalyzes the interconversion between

FIG 5 Legend (Continued)

incubated with 40 mg/liter tobramycin-Texas Red (TbTR) for 30 min. The bacteria were collected by centrifugation and washed three times with PBS, followed by lysis in PBS by sonication. The fluorescence was measured with a luminometer. The relative fluorescence was normalized by the corresponding total protein concentration. Data represent the mean \pm standard deviation of the results from three samples. **, $P < 0.01$; ***, $P < 0.001$ by Student's *t* test.

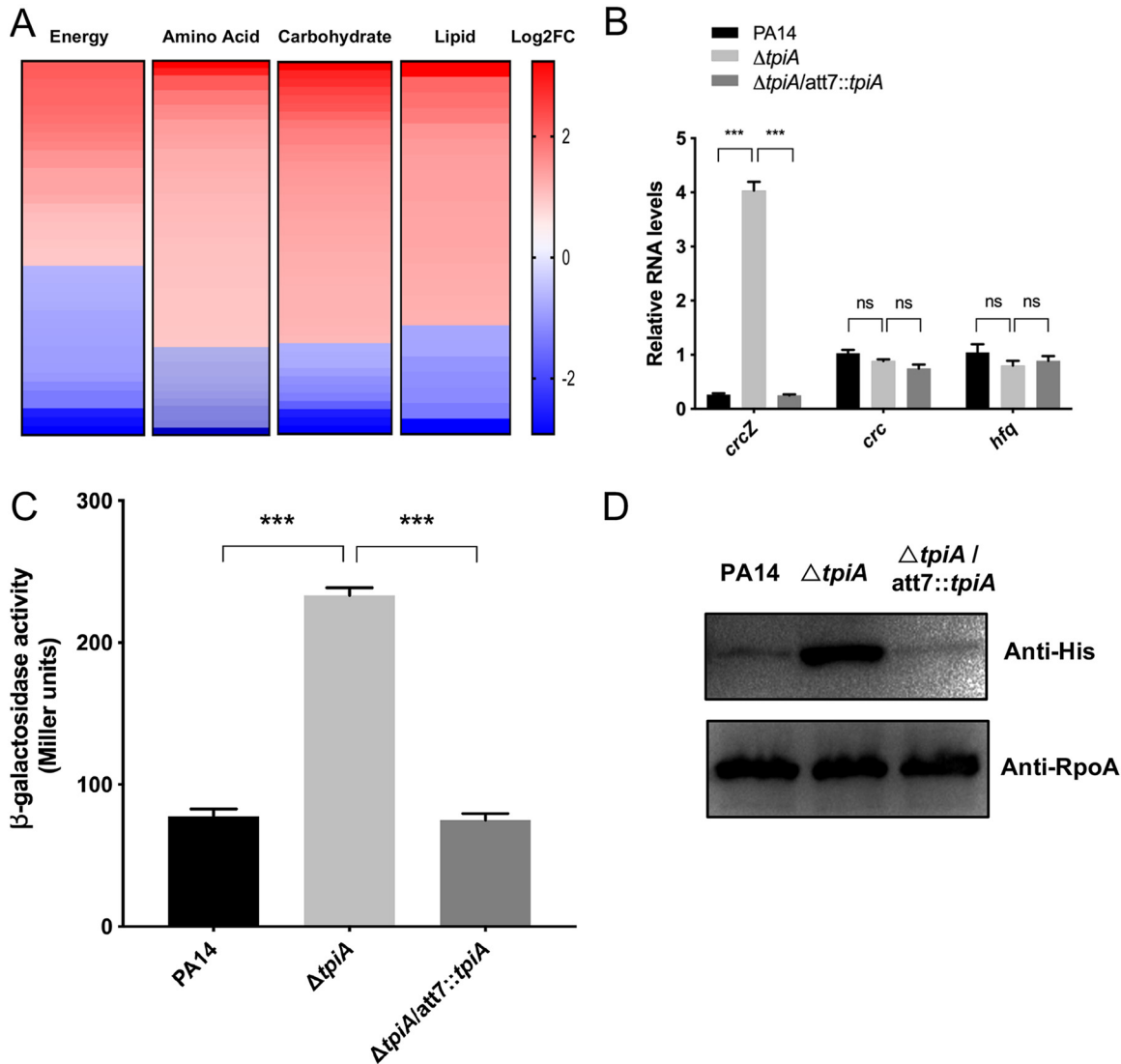


FIG 6 Mutation of the *tpiA* gene affects the expression of metabolic genes. (A) RNA sequencing (RNA-seq) results. Values are reported as log₂ fold change (Log₂FC) of the expression of energy metabolism, amino acid metabolism, carbohydrate metabolism, and lipid metabolism genes in the $\Delta tpiA$ mutant over wild-type PA14. (B) The bacteria were cultured in LB to an OD₆₀₀ of 1. The RNA levels of *crc*, *hfq*, and *crcZ* were determined by real-time PCR. The 30S ribosomal protein gene *rpsL* was used as an internal control. Data represent the mean \pm standard deviation of the results from three samples. ***, $P < 0.001$ by Student's *t* test. (C) Indicated strains containing the *amiE*-*lacZ* translation fusion were cultured in LB with 1 mM isopropyl- β -D-thiogalactopyranoside (IPTG). When the OD₆₀₀ reached 1, the bacteria were collected, followed by the β -galactosidase activity assay. Data represent the mean \pm standard deviation of the results from three samples. ***, $P < 0.001$ by Student's *t* test. (D) Indicated strains containing the *amiE*-His translational fusion were cultured in LB with 0.2% L-arabinose. When the OD₆₀₀ reached 1, the bacteria were collected. The *AmiE*-His levels were determined by Western blotting with RpoA as the loading control.

G3P and DHAP, an important reaction in glycolysis and gluconeogenesis. We suspected that without TpiA, the pyruvate generated from glycolysis cannot be converted into DHAP, thus breaking off the flux of carbon toward the phospholipid synthesis while increasing the TCA cycle. On the other hand, DHAP generated from glycerol cannot be directly converted into G3P in the $\Delta tpiA$ mutant, which might hinder gluconeogenesis. Overall, these results suggest a critical role of TpiA in carbon metabolism in *P. aeruginosa*.

Perturbations in metabolism have been found to influence bacterial virulence and resistance to antibiotics. The pyruvate dehydrogenase genes *aceAB* are required for expression of the T3SS genes (36). Histidine and tryptophan utilization have been found to interfere with the T3SS in *P. aeruginosa* (37, 38). CbrA and CbrB compose a

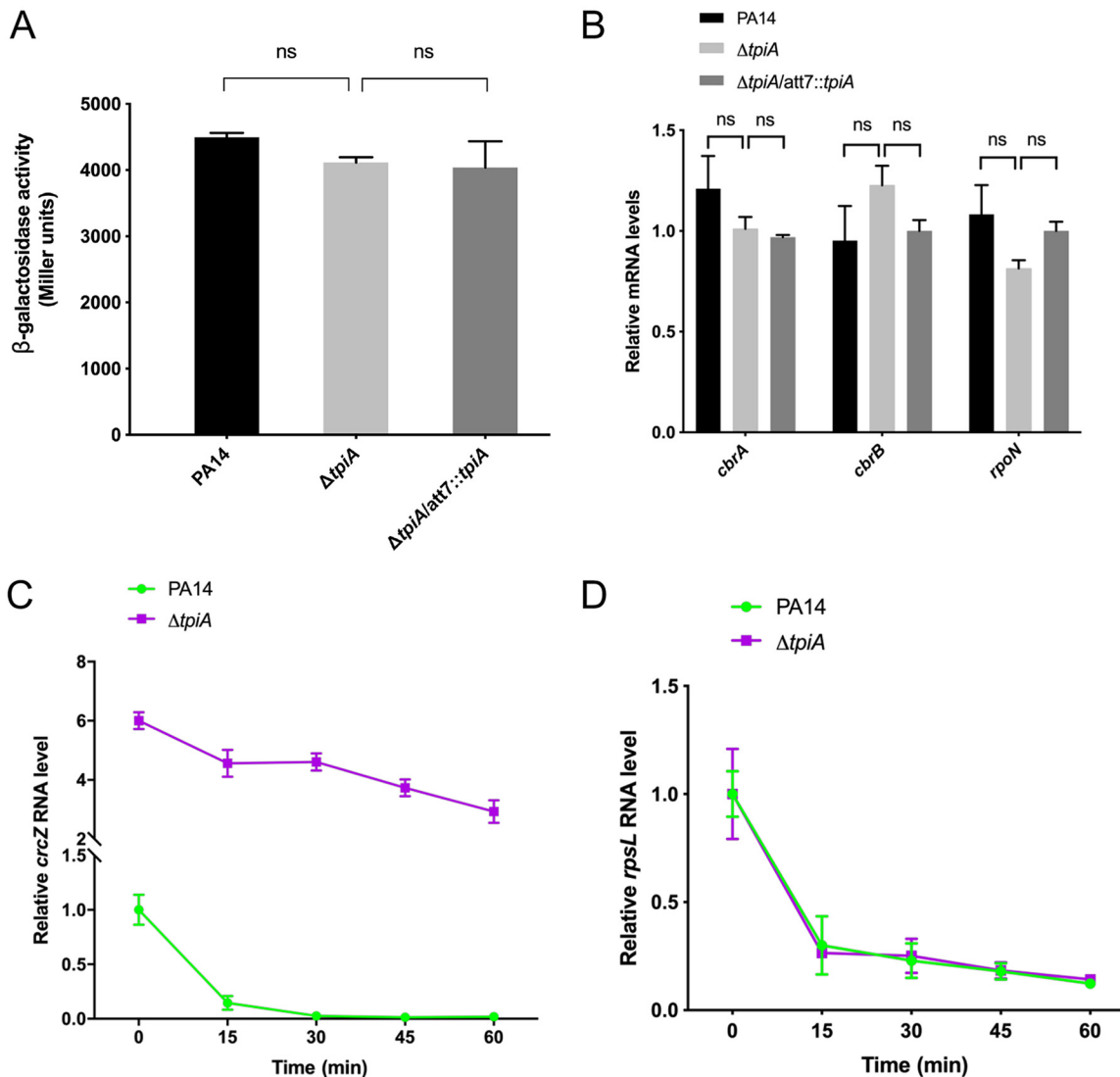


FIG 7 Mutation of the *tpiA* gene increases the stability of CrcZ. (A) PA14, the $\Delta tpiA$ mutant, and the complemented strain containing the P_{crcZ} -*lacZ* transcriptional fusion were cultured in LB to an OD_{600} of 1. The bacteria were collected, followed by the β -galactosidase activity assay. (B) The indicated strains were cultured in LB to an OD_{600} of 1. The mRNA levels of *cbrA*, *cbrB*, and *rpoN* were determined by real-time PCR. The 30S ribosomal protein gene *rpsL* was used as an internal control. Data represent the mean \pm standard deviation of the results from three samples. ns, not significant. (C and D) Degradation of CrcZ (C) and the *rpsL* mRNA (D) in wild-type PA14 and the $\Delta tpiA$ mutant. Bacterial cells were treated with rifampin, and at the indicated time points, the bacteria were collected and mixed with equal numbers of *gfp*-expressing *E. coli* cells. Total RNA was isolated, and the relative RNA levels were determined by real-time PCR. The *gfp* RNA level in each sample was used as the internal control for normalization.

two-component regulatory system that regulates genes involved in carbon and nitrogen utilization. Mutation of *cbrA* results in defective swarming motility, enhanced cytotoxicity and biofilm formation, and increased antibiotic resistance (39). The CbrA/CbrB system directly regulates the expression of the small RNA (sRNA) CrcZ, which antagonizes the Crc/Hfq-mediated CCR (9, 40). Crc is required for the twitching motility, biofilm formation, and expression of the T3SS and quorum sensing system genes, and it contributes to bacterial resistance to various antibiotics (41, 42). Here, we found that the CrcZ level was increased in the $\Delta tpiA$ mutant. The *cbrA* and *cbrB* mRNA levels and the *crcZ* promoter activity were similar in the $\Delta tpiA$ mutant and wild-type PA14, indicating a similar level of the CbrA ligand. We further demonstrated that CrcZ stability was increased in the $\Delta tpiA$ mutant. We suspected that mutation of *tpiA* alters the intracellular metabolite intermediate levels as well as the redox status, which might affect RNase levels and activities (43, 44). Deletion of *crcZ* in the $\Delta tpiA$ mutant back-

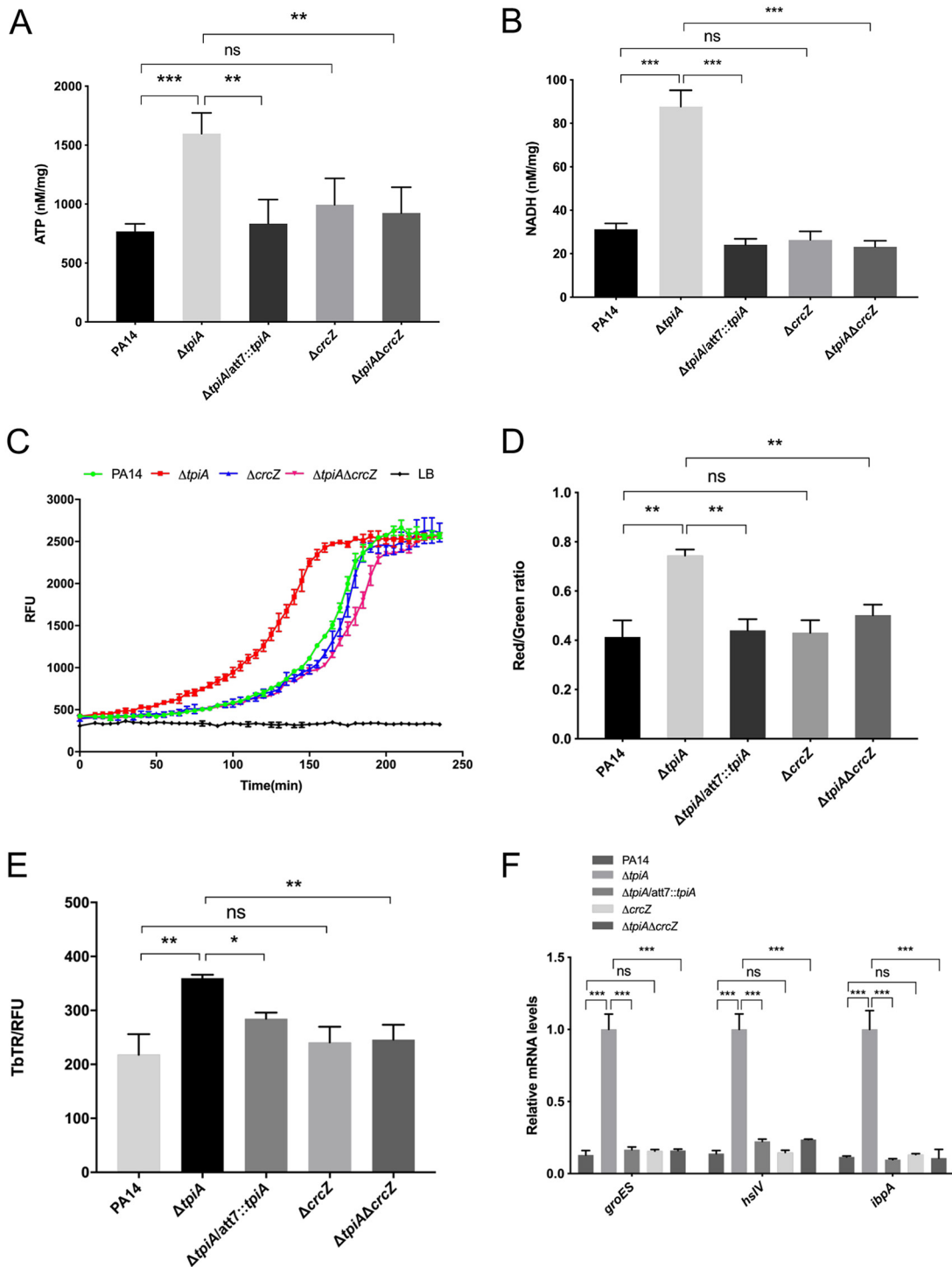


FIG 8 The increased level of CrcZ in the $\Delta tpiA$ mutant contributes to the hypersusceptibility to tobramycin. (A) The intracellular ATP levels were determined using the enhanced ATP assay kit. Bacteria were cultured in LB medium at 37°C to OD₆₀₀ of 1. A volume of 1.5 ml of the bacteria was collected and lysed by ultrasound sonication. Measurement of the ATP level in the supernatant was performed according to the manufacturer's instruction. Total protein levels were quantified by BCA analysis for normalization. Data represent the mean \pm standard deviation of the results from three samples. **, $P < 0.01$; ***, $P < 0.001$ by Student's t test. (B) The intracellular NADH levels were determined using an Amplitude fluorimetric NAD/NADH ratio assay kit. Bacteria were cultured in LB medium at 37°C to an OD₆₀₀ of 1. The bacteria were lysed in PBS by sonication. Measurement of the NADH level in the supernatant was performed according to the manufacturer's instruction. Total proteins were quantified by the BCA analysis for normalization. Data represent the mean \pm standard deviation of the results from three samples. **, $P < 0.01$ by Student's t test. (C) ETC activity was quantified by an extracellular oxygen consumption assay kit. A total of 1.5×10^5 bacterial cells in fresh LB were mixed with 10 μ l of the O₂ consumption reagent in a black 96-well plate and sealed with 50 μ l mineral oil to isolate the air. The fluorescences were measured every 5 min for 4 h. (D) Quantification of PMF-dependent membrane potential

(Continued on next page)

TABLE 4 MICs of the aminoglycoside antibiotics against indicated strains in MHB

Strain	MIC ($\mu\text{g/ml}$) ^a				
	GEN	TOB	NEO	STR	AMK
PA14	1	1	16	16	8
ΔtpiA mutant	0.25	0.125	4	4	2
$\Delta\text{tpiA}/\text{att7}::\text{tpiA}$ mutant	1	1	16	16	8
ΔcrcZ mutant	1	1	16	16	8
ΔtpiA ΔcrcZ mutant	1	1	16	16	8

^aGEN, gentamicin; TOB, tobramycin; NEO, neomycin; STR, streptomycin; AMK, amikacin.

ground restored the expression of the T3SS genes and bacterial cytotoxicity, suggesting an important role of CrcZ in repression of the T3SS in the ΔtpiA mutant. Recent studies have demonstrated that enhancing bacterial metabolic activity increases the bactericidal effect of antibiotics. For instance, exogenous glutamate stimulates metabolic flux through the pyruvate cycle (P cycle), which increases the aminoglycoside killing efficacy in *Escherichia coli* and *Edwardsiella tarda* (32). Supplementation of central carbon metabolites, such as fumarate, succinate, and citrate, increases the susceptibility of *P. aeruginosa* to tobramycin. The exogenous carbon sources enhance bacterial respiration, thereby increasing membrane potential and the uptake of antibiotics (13, 19, 45–47). Our results revealed that mutation of *tpiA* increased the bacterial respiration and uptake of tobramycin, presumably due to the aberrant carbon flux into the TCA cycle. Therefore, inhibition of TpiA might increase the bacterial killing efficacy of tobramycin and simultaneously decrease bacterial virulence, making TpiA a potential drug target.

MATERIALS AND METHODS

Bacterial strains and plasmids. The bacterial strains, plasmids, and primers used in this study are listed in Table S4. To construct the *tpiA* deletion mutant, a 1,087-bp fragment and a 1,511-bp fragment upstream and downstream of the *tpiA* coding region, respectively, were amplified by PCR using the PA14 chromosome as the template and the primers listed in Table S4. The fragments were cloned into the plasmid pEX18Tc (48). Deletion of the *tpiA* gene in *P. aeruginosa* was performed as previously described (48). The ΔcrcZ mutant was constructed by the same method. For the complementation of *tpiA*, the *tpiA* gene and its native promoter were amplified using the primers shown in Table S4. The fragments were ligated into pUC18T-mini-Tn7T-Gm. Integration of the *tpiA* fragment into the bacterial chromosome and removal of the gentamicin resistant cassette were performed as previously described (49).

Bacteria were cultured in LB medium at 37°C. Antibiotics were used at the following concentrations: for *E. coli*, 10 $\mu\text{g ml}^{-1}$ tetracycline, 100 $\mu\text{g ml}^{-1}$ ampicillin, and 10 $\mu\text{g ml}^{-1}$ gentamicin; and for *P. aeruginosa*, 50 $\mu\text{g ml}^{-1}$ gentamicin, 50 $\mu\text{g ml}^{-1}$ tetracycline, and 150 $\mu\text{g ml}^{-1}$ carbenicillin.

The basic artificial sputum medium (ASM) is composed of 5 g mucin from pig stomach mucosa (NBS Biologicals), 5.9 mg diethylenetriaminepentaacetic acid (DTPA) (Sigma), 4 g low-molecular-weight salmon sperm DNA (Fluka), 1.81 g Tris base (Sigma), 2.2 g KCl, 5 g NaCl, 5 ml egg yolk emulsion (Oxoid), and 5 g Casamino Acids (Difco) per 1 liter of water (pH 7.0).

The maximum growth rate (MGR) was calculated as $(W7 - W4)/3$, where W7 and W4 represent the bacterial OD₆₀₀ at 7 h and 4 h, respectively.

Antibiotic susceptibility test. The MIC was determined using broth microdilution in accordance with Clinical and Laboratory Standards Institute (CLSI) recommendations (<http://iaclid.org/DL/public/CLSI-2018-M100-S28.pdf>). Each well of the 96-well microtiter plate was filled with 0.1 ml Mueller-Hinton broth (MHB) with serially diluted concentrations of the individual antibiotics. Then, 0.1 ml bacterial culture (5×10^5 CFU) was inoculated into each well and incubated at 37°C for 20 h. MICs were recorded as the lowest concentration of antibiotic inhibiting visible growth. The same procedure

FIG 8 Legend (Continued)

DiOC₂(3). The logarithmic-phase bacterial cells were incubated with DiOC₂(3) for 1 h and then subjected to flow cytometry analysis. Data represent the mean \pm standard deviation of the results from three samples. **, $P < 0.01$ by Student's *t* test. (E) The internalization of tobramycin was quantified by Texas Red-labeled tobramycin (TbTR). The bacteria were cultured in LB to an OD₆₀₀ of 1, followed by incubation with 40 mg/liter TbTR for 30 min. The bacteria were collected by centrifugation and washed three times with PBS and then lysed in PBS by sonication. The Texas Red was excited at 595 nm, and the emission at 615 nm was measured with a luminometer. The relative fluorescence was normalized by the total protein. Data represent the mean \pm standard deviation of the results from three samples. *, $P < 0.05$; **, $P < 0.01$; ns, not significant by Student's *t* test. (F) The bacteria were treated with 0.1 mg/liter tobramycin for 30 min, followed by RNA isolation. The mRNA levels of *groES*, *hslV*, and *ibpA* were determined by real-time PCR. The 30S ribosomal protein gene *rpsL* was used as an internal control. Data represent the mean \pm standard deviation of the results from three samples. **, $P < 0.01$ by Student's *t* test.

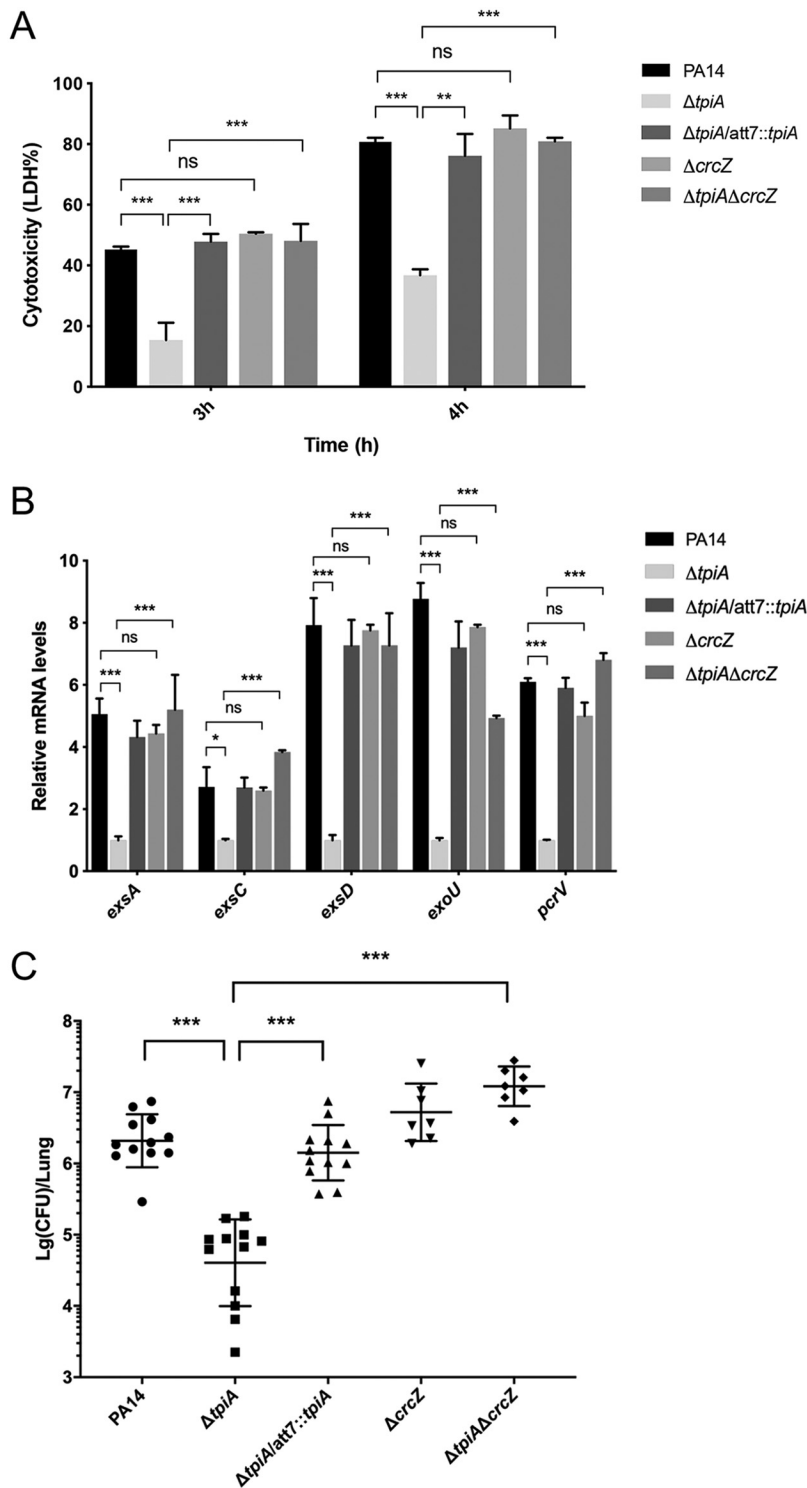


FIG 9 CrcZ represses the T3SS in the $\Delta tpiA$ mutant. (A) A549 cells were infected with the indicated strains at a multiplicity of infection (MOI) of 50 for 4 h. The relative cytotoxicity was determined by the LDH release assay. Data represent the mean \pm standard deviation of the results from three samples. (B) Indicated strains were grown with 5 mM EGTA for 4 h. The relative mRNA levels of the T3SS genes were determined by real-time PCR. The 30S ribosomal protein gene *rpsL* was used as the internal control. Data represent the mean \pm standard deviation of the results from three samples. **, $P < 0.01$; ns, not significant by Student's *t* test. (C) Mice were infected intranasally with the indicated strains. At 12 h postinfection, lungs from the infected mice were isolated. Bacterial loads were determined by serial dilution and plating. Each group of 12 mice was infected with the strain of wild-type PA14, $\Delta tpiA$ mutant, or $\Delta tpiA/att7::tpiA$ mutant. Each group of 7 mice was infected with the $\Delta crcZ$ mutant or the $\Delta tpiA \Delta crcZ$ mutant. ***, $P < 0.001$ by Student's *t* test.

was used to determine the MICs in ASM. All of the MICs of the strains were tested at least three times.

Transcriptome sequencing and analysis. Bacteria were cultured in LB medium at 37°C until late-logarithmic phase (OD_{600} 1). Total RNA was isolated using the RNAprep pure cell/bacteria kit (Tiangen Biotec, Beijing, China). Two replicates were prepared for each strain. Sequencing and analysis services were performed as previously described (50). The detailed method is described in Text S1 in the supplemental material.

Real-time PCR. Total bacterial RNA was isolated using the RNAprep pure cell/bacteria kit (Tiangen Biotec, Beijing, China). cDNAs were synthesized with a reverse transcriptase and random primers (TaKaRa, Dalian, China). Real-time PCR was performed using the SYBR II green supermix (Bio-Rad, Beijing, China). The 30S ribosomal protein gene *rpsL* was used as the internal control.

Measurement of the intracellular DHAP level. Bacterial intracellular DHAP levels were determined using a high-sensitivity dihydroxyacetone phosphate assay kit (catalog no. MAK275; Sigma-Aldrich, USA). Bacteria were cultured in M9 medium with 20 mM glucose and 40 mM glycerol as the carbon sources at 37°C to an OD_{600} of 1. Then, the bacteria were washed three times with phosphate-buffered saline (PBS) and incubated in M9 medium with 40 mM glucose or 80 mM glycerol as the sole carbon source for 1 h. The bacterial cells were lysed in the PBS buffer by sonication. Measurement of the DHAP level in the supernatant was performed according to the manufacturer's instructions. The standard curve was prepared using a standard DHAP provided by the kit. The total protein level was quantified using a bicinchoninic acid (BCA) analysis kit (Beyotime, Shanghai, China).

Tobramycin-Texas Red uptake assay. Tobramycin was conjugated to Texas Red as previously described (19, 51). Briefly, 1 μ g Texas Red sulfonyl chloride was dissolved in 50 μ l anhydrous *N,N*-dimethyl formamide on ice. Then, the solution was added slowly to 2.3 ml of 0.1 M K_2CO_3 (pH 8.5) with or without 10 mg/ml tobramycin. To quantify the uptake of the tobramycin-Texas Red (TbTR), bacteria were grown in LB to an OD_{600} of 1 and then incubated with 40 mg/liter TbTR or Texas Red for 30 min. The bacteria were collected by centrifugation and washed three times with PBS. The bacterial cells were lysed in PBS by sonication. The Texas Red was excited at 595 nm, and the emission at 615 nm (19, 51) was measured with a luminometer (Varioskan Flash; Thermo Scientific). Total bacterial protein concentrations were quantified using a BCA analysis for calibration.

Bacterial ATP level assay. The intracellular ATP levels were determined using an enhanced ATP assay kit (Beyotime Biotec, Shanghai, China). Bacteria were cultured in LB medium at 37°C until late-logarithmic phase (OD_{600} 1). Bacterial cells in 1.5 ml culture were collected by centrifugation and resuspended using the lysis buffer provided by the kit. The cells were broken by ultrasound sonication. Then, the cell debris was removed by centrifugation. One hundred microliters of the ATP detection working fluid was mixed with 20 μ l of the bacterial supernatant. Chemiluminescence was detected with a luminometer (Varioskan Flash; Thermo Scientific). Total proteins were quantified by the BCA analysis for calibration. Standard curves were prepared using the standard ATP samples provided by the kit.

Bacterial NADH level assay. Bacterial NADH levels were determined using an Amplitude fluorimetric NAD/NADH ratio assay kit (AAT Bioquest, Inc., USA). Bacteria were cultured in LB medium at 37°C to an OD_{600} of 1. The bacterial cells were lysed in PBS by sonication. Measurement of the NADH level in the supernatant was performed according to the manufacturer's instructions. The standard curve was prepared using the NADH provided by the kit. The total protein level was quantified using a BCA analysis kit (Beyotime, Shanghai, China).

Membrane potential assay. The bacteria were cultured at 37°C in LB medium to an OD_{600} of 1. The bacteria were diluted to 10^6 CFU/ml in PBS. To each 1.5 ml of the bacterial suspension, 2 μ l of 20 mM DiOC₂(3) was added and incubated for 1 h at 37°C in dark, followed by flow cytometry analysis (Accuri C6; BD). The DiOC₂(3) was excited at 484 nm, and the emissions at 530 nm (green fluorescence) and 610 nm (red fluorescence) were measured. Cells without staining were subjected to the fluorescence measurement, and the values were subtracted from those of the corresponding cells with DiOC₂(3) staining. All experiments were performed at least in triplicate. The green fluorescence is relatively independent of membrane potential and mainly reflects particle sizes, while the red fluorescence is highly dependent on membrane potential and particle sizes. Membrane potential was indicated by the ratio of the green to red fluorescence (30).

Oxygen consumption assay. Bacterial oxygen consumption was determined using an extracellular oxygen consumption assay kit (Abcam), according to the manufacturer's instructions. Briefly, overnight bacterial cultures were diluted 1:100 in fresh LB medium and grown at 37°C until the OD_{600} reached 1. The bacterial concentration was adjusted to 1×10^6 CFU/ml in fresh LB medium. One hundred fifty microliters of the bacterial resuspension was transferred to each well of a 96-well plate that contained 10 μ l of O₂ consumption reagent. Each well was sealed with 50 μ l mineral oil provided by the kit to isolate the air. The dye excites at 380 nm and emits at 650 nm, and the signal was monitored with a luminometer (Varioskan Flash; Thermo Scientific).

β -Galactosidase assay. Overnight bacterial cultures were diluted 1:100 in fresh LB and grown at 37°C until the OD_{600} reached 1. Bacterial cells in 0.5 ml culture were collected and resuspended in 1.5 ml Z buffer (60 mM Na₂HPO₄, 60 mM NaH₂PO₄, 1 mM MgSO₄, 10 mM KCl, 50 mM β -mercaptoethanol [pH 7.0]). The β -galactosidase activity was determined as previously described (52).

RNA stability analysis. *P. aeruginosa* strains were grown in LB at 37°C to an OD_{600} of 1. Then, the bacteria were treated with 100 μ g/ml rifampin to stop transcription. At each indicated time point, the bacterial cells were taken and mixed with an equal number of *E. coli* cells expressing the *gfp* gene. Total RNA was purified, and the levels of *crcZ* were analyzed by real-time PCR. The *gfp* RNA level was used as an internal control for normalization.

Cytotoxicity assay. Cytotoxicity was determined using a lactate dehydrogenase (LDH) release assay. The human lung carcinoma cell line A549 cells were cultured in Dulbecco's modified Eagle medium with 2% (vol/vol) heat-inactivated fetal bovine serum at 37°C with 5% CO₂. A total of 2×10^5 cells were seeded into each well of a 24-well plate and cultured overnight. The bacterial cells were cultured at 37°C in LB medium to an OD₆₀₀ of 1 and then washed twice with PBS and resuspended in PBS. After the addition of the bacteria to each well, the plate was centrifuged at $700 \times g$ for 10 min to synchronize the infection. Four hours postinfection, LDH in the medium was measured using the LDH cytotoxicity assay kit (Beyotime, Shanghai, China). Cells treated with the LDH release buffer provided by the kit were used as the control for the total LDH. The cytotoxicity percentage was calculated according to the manufacturer's instructions.

Murine acute pneumonia model. The animal infection experiments were performed following the National and Nankai University guidelines on the use of animals in research. The protocol (permit number NK-04-2012) was approved by the animal care and use committee of the College of Life Sciences of Nankai University. The infection of mice was performed as previously described (53). Briefly, overnight bacterial culture was diluted 1:100 in fresh LB and grown at 37°C until the OD₆₀₀ reached 1. The collected bacterial cells were washed once with PBS. The bacterial concentration was adjusted to 2×10^8 CFU/ml in PBS. Each female BALB/c mouse (Vital River, Beijing, China) at the age of 6 to 8 weeks was anesthetized with an intraperitoneal injection of 100 μ l of 7.5% chloral hydrate, followed by inoculation with 20 μ l of the bacterial suspension, resulting in 4×10^6 CFU per mouse. Twelve hours postinfection, the mice were sacrificed. Lungs were isolated and subjected to homogenization. The bacterial load in each lung was determined by plating.

SUPPLEMENTAL MATERIAL

Supplemental material is available online only.

TEXT S1, DOCX file, 0.1 MB.

FIG S1, PDF file, 0.1 MB.

FIG S2, PDF file, 0.1 MB.

FIG S3, PDF file, 0.2 MB.

FIG S4, PDF file, 0.1 MB.

TABLE S1, DOCX file, 0.1 MB.

TABLE S2, DOCX file, 0.1 MB.

TABLE S3, XLS file, 0.1 MB.

TABLE S4, DOCX file, 0.1 MB.

ACKNOWLEDGMENTS

This work was supported by the National Key Research and Development Project of China (grant 2017YFE0125600), National Science Foundation of China (grants 31670130, 31970680, 31870130, and 81670766), Tianjin Municipal Science and Technology Commission, China (grant 19JCYBJC24700), and the "Fundamental Research Funds for the Central Universities," Nankai University (grants 63191521 and 63191121).

The funders had no role in the study design, data collection and interpretation, or the decision to submit the work for publication.

REFERENCES

- Driscoll JA, Brody SL, Kollef MH. 2007. The epidemiology, pathogenesis and treatment of *Pseudomonas aeruginosa* infections. *Drugs* 67:351–368. <https://doi.org/10.2165/00003495-200767030-00003>.
- Sawa T. 2014. The molecular mechanism of acute lung injury caused by *Pseudomonas aeruginosa*: from bacterial pathogenesis to host response. *J Intensive Care* 2:10. <https://doi.org/10.1186/2052-0492-2-10>.
- Hauser AR. 2009. The type III secretion system of *Pseudomonas aeruginosa*: infection by injection. *Nat Rev Microbiol* 7:654–665. <https://doi.org/10.1038/nrmicro2199>.
- Mah TF, O'Toole GA. 2001. Mechanisms of biofilm resistance to antimicrobial agents. *Trends Microbiol* 9:34–39. [https://doi.org/10.1016/S0966-842X\(00\)01913-2](https://doi.org/10.1016/S0966-842X(00)01913-2).
- Hall CW, Mah TF. 2017. Molecular mechanisms of biofilm-based antibiotic resistance and tolerance in pathogenic bacteria. *FEMS Microbiol Rev* 41:276–301. <https://doi.org/10.1093/femsre/fux010>.
- Lister PD, Wolter DJ, Hanson ND. 2009. Antibacterial-resistant *Pseudomonas aeruginosa*: clinical impact and complex regulation of chromosomally encoded resistance mechanisms. *Clin Microbiol Rev* 22:582–610. <https://doi.org/10.1128/CMR.00040-09>.
- Li XZ, Plesiat P, Nikaido H. 2015. The challenge of efflux-mediated antibiotic resistance in Gram-negative bacteria. *Clin Microbiol Rev* 28:337–418. <https://doi.org/10.1128/CMR.00117-14>.
- Rojas F. 2010. Carbon catabolite repression in *Pseudomonas*: optimizing metabolic versatility and interactions with the environment. *FEMS Microbiol Rev* 34:658–684. <https://doi.org/10.1111/j.1574-6976.2010.00218.x>.
- Sonnleitner E, Wulf A, Campagne S, Pei XY, Wolfinger MT, Forlani G, Prindl K, Abdou L, Resch A, Allain FH, Luisi BF, Urlaub H, Blasi U. 2018. Interplay between the catabolite repression control protein Crc, Hfq and RNA in Hfq-dependent translational regulation in *Pseudomonas aeruginosa*. *Nucleic Acids Res* 46:1470–1485. <https://doi.org/10.1093/nar/gkx1245>.
- Zhang XX, Rainey PB. 2008. Dual involvement of CbrAB and NtrBC in the regulation of histidine utilization in *Pseudomonas fluorescens* SBW25. *Genetics* 178:185–195. <https://doi.org/10.1534/genetics.107.081984>.
- Sonnleitner E, Abdou L, Haas D. 2009. Small RNA as global regulator of carbon catabolite repression in *Pseudomonas aeruginosa*. *Proc Natl Acad Sci U S A* 106:21866–21871. <https://doi.org/10.1073/pnas.pnas.0910308106>.
- Sonnleitner E, Blasi U. 2014. Regulation of Hfq by the RNA CrcZ in

- Pseudomonas aeruginosa* carbon catabolite repression. *PLoS Genet* 10: e1004440. <https://doi.org/10.1371/journal.pgen.1004440>.
13. Dong YH, Zhang XF, Zhang LH. 2013. The global regulator Crc plays a multifaceted role in modulation of type III secretion system in *Pseudomonas aeruginosa*. *Microbiol Open* 2:161–172. <https://doi.org/10.1002/mbo3.54>.
 14. Yang N, Ding S, Chen F, Zhang X, Xia Y, Di H, Cao Q, Deng X, Wu M, Wong CC, Tian XX, Yang CG, Zhao J, Lan L. 2015. The Crc protein participates in down-regulation of the Lon gene to promote rhamnolipid production and rhl quorum sensing in *Pseudomonas aeruginosa*. *Mol Microbiol* 96:526–547. <https://doi.org/10.1111/mmi.12954>.
 15. Pusic P, Tata M, Wolfinger MT, Sonnleitner E, Haussler S, Blasi U. 2016. Cross-regulation by CrcZ RNA controls anoxic biofilm formation in *Pseudomonas aeruginosa*. *Sci Rep* 6:39621. <https://doi.org/10.1038/srep39621>.
 16. Pusic P, Sonnleitner E, Krennmayr B, Heitzinger DA, Wolfinger MT, Resch A, Blasi U. 2018. Harnessing metabolic regulation to increase Hfq-dependent antibiotic susceptibility in *Pseudomonas aeruginosa*. *Front Microbiol* 9:2709. <https://doi.org/10.3389/fmicb.2018.02709>.
 17. Vitko NP, Spahich NA, Richardson AR. 2015. Glycolytic dependency of high-level nitric oxide resistance and virulence in *Staphylococcus aureus*. *mBio* 6:e00045-15. <https://doi.org/10.1128/mBio.00045-15>.
 18. Vilch e C, Hartman T, Weinrick B, Jain P, Weisbrod TR, Leung LW, Freundlich JS, Jacobs WR, Jr. 2017. Enhanced respiration prevents drug tolerance and drug resistance in *Mycobacterium tuberculosis*. *Proc Natl Acad Sci U S A* 114:4495–4500. <https://doi.org/10.1073/pnas.1704376114>.
 19. Meylan S, Porter CBM, Yang JH, Belenky P, Gutierrez A, Lobritz MA, Park J, Kim SH, Moskowitz SM, Collins JJ. 2017. Carbon sources tune antibiotic susceptibility in *Pseudomonas aeruginosa* via tricarboxylic acid cycle control. *Cell Chem Biol* 24:195–206. <https://doi.org/10.1016/j.chembiol.2016.12.015>.
 20. Liberati NT, Urbach JM, Miyata S, Lee DG, Drenkard E, Wu G, Villanueva J, Wei T, Ausubel FM. 2006. An ordered, nonredundant library of *Pseudomonas aeruginosa* strain PA14 transposon insertion mutants. *Proc Natl Acad Sci U S A* 103:2833–2838. <https://doi.org/10.1073/pnas.0511100103>.
 21. Fuhrer T, Fischer E, Sauer U. 2005. Experimental identification and quantification of glucose metabolism in seven bacterial species. *J Bacteriol* 187:1581–1590. <https://doi.org/10.1128/JB.187.5.1581-1590.2005>.
 22. Kohlstedt M, Wittmann C. 2019. GC-MS-based ¹³C metabolic flux analysis resolves the parallel and cyclic glucose metabolism of *Pseudomonas putida* KT2440 and *Pseudomonas aeruginosa* PAO1. *Metab Eng* 54:35–53. <https://doi.org/10.1016/j.ymben.2019.01.008>.
 23. Tavares IM, Leitao JH, Sa-Correia I. 2003. Chromosomal organization and transcription analysis of genes in the vicinity of *Pseudomonas aeruginosa* *glmM* gene encoding phosphoglucosamine mutase. *Biochem Biophys Res Commun* 302:363–371. [https://doi.org/10.1016/s0006-291x\(03\)00169-4](https://doi.org/10.1016/s0006-291x(03)00169-4).
 24. Wright EA, Fothergill JL, Paterson S, Brockhurst MA, Winstanley C. 2013. Sub-inhibitory concentrations of some antibiotics can drive diversification of *Pseudomonas aeruginosa* populations in artificial sputum medium. *BMC Microbiol* 13:170. <https://doi.org/10.1186/1471-2180-13-170>.
 25. Kirchner S, Fothergill JL, Wright EA, James CE, Mowat E, Winstanley C. 2012. Use of artificial sputum medium to test antibiotic efficacy against *Pseudomonas aeruginosa* in conditions more relevant to the cystic fibrosis lung. *J Vis Exp* 64:e3857. <https://doi.org/10.3791/3857>.
 26. Kindrachuk KN, Fernandez L, Bains M, Hancock RE. 2011. Involvement of an ATP-dependent protease, PA0779/AsrA, in inducing heat shock in response to tobramycin in *Pseudomonas aeruginosa*. *Antimicrob Agents Chemother* 55:1874–1882. <https://doi.org/10.1128/AAC.00935-10>.
 27. Hocquet D, Vogne C, El Garch F, Vejux A, Gotoh N, Lee A, Lomovskaya O, Pl siat P. 2003. MexXY-OprM efflux pump is necessary for a adaptive resistance of *Pseudomonas aeruginosa* to aminoglycosides. *Antimicrob Agents Chemother* 47:1371–1375. <https://doi.org/10.1128/aac.47.4.1371-1375.2003>.
 28. Morita Y, Tomida J, Kawamura Y. 2012. MexXY multidrug efflux system of *Pseudomonas aeruginosa*. *Front Microbiol* 3:408. <https://doi.org/10.3389/fmicb.2012.00408>.
 29. Taber HW, Mueller JP, Miller PF, Arrow AS. 1987. Bacterial uptake of aminoglycoside antibiotics. *Microbiol Rev* 51:439–457.
 30. Novo D, Perlmutter NG, Hunt RH, Shapiro HM. 1999. Accurate flow cytometric membrane potential measurement in bacteria using diethylloxycarbocyanine and a ratiometric technique. *Cytometry* 35:55–63. [https://doi.org/10.1002/\(SICI\)1097-0320\(19990101\)35:1<55::AID-CYTO8>3.0.CO;2-2](https://doi.org/10.1002/(SICI)1097-0320(19990101)35:1<55::AID-CYTO8>3.0.CO;2-2).
 31. Jackson AA, Gross MJ, Daniels EF, Hampton TH, Hammond JH, Vallet-Gely I, Dove SL, Stanton BA, Hogan DA. 2013. Anr and its activation by PlcH activity in *Pseudomonas aeruginosa* host colonization and virulence. *J Bacteriol* 195:3093–3104. <https://doi.org/10.1128/JB.02169-12>.
 32. Su YB, Peng B, Li H, Cheng ZX, Zhang TT, Zhu JX, Li D, Li MY, Ye JZ, Du CC, Zhang S, Zhao XL, Yang MJ, Peng XX. 2018. Pyruvate cycle increases aminoglycoside efficacy and provides respiratory energy in bacteria. *Proc Natl Acad Sci U S A* 115:E1578–E1587. <https://doi.org/10.1073/pnas.1714645115>.
 33. Corona F, Martinez JL, Nickel PI. 2019. The global regulator Crc orchestrates the metabolic robustness underlying oxidative stress resistance in *Pseudomonas aeruginosa*. *Environ Microbiol* 21:898–912. <https://doi.org/10.1111/1462-2920.14471>.
 34. Pei XY, Dendooven T, Sonnleitner E, Chen S, Blasi U, Luisi BF. 2019. Architectural principles for Hfq/Crc-mediated regulation of gene expression. *Elife* 8:e43158. <https://doi.org/10.7554/eLife.43158>.
 35. Xu Y, Liu F, Chen S, Wu J, Hu Y, Zhu B, Sun Z. 2018. In vivo evolution of drug-resistant *Mycobacterium tuberculosis* in patients during long-term treatment. *BMC Genomics* 19:640. <https://doi.org/10.1186/s12864-018-5010-5>.
 36. Dacheux D, Epaulard O, de Groot A, Guery B, Leberre R, Attree I, Polack B, Toussaint B. 2002. Activation of the *Pseudomonas aeruginosa* type III secretion system requires an intact pyruvate dehydrogenase aceAB operon. *Infect Immun* 70:3973–3977. <https://doi.org/10.1128/iai.70.7.3973-3977.2002>.
 37. Rietsch A, Wolfgang MC, Mekalanos JJ. 2004. Effect of metabolic imbalance on expression of type III secretion genes in *Pseudomonas aeruginosa*. *Infect Immun* 72:1383–1390. <https://doi.org/10.1128/iai.72.3.1383-1390.2004>.
 38. Shen DK, Filopon D, Chaker H, Boullanger S, Derouazi M, Polack B, Toussaint B. 2008. High-cell-density regulation of the *Pseudomonas aeruginosa* type III secretion system: implications for tryptophan catabolites. *Microbiology* 154:2195–2208. <https://doi.org/10.1099/mic.0.2007/013680-0>.
 39. Yeung AT, Bains M, Hancock RE. 2011. The sensor kinase CbrA is a global regulator that modulates metabolism, virulence, and antibiotic resistance in *Pseudomonas aeruginosa*. *J Bacteriol* 193:918–931. <https://doi.org/10.1128/JB.00911-10>.
 40. Abdou L, Chou HT, Haas D, Lu CD. 2011. Promoter recognition and activation by the global response regulator CbrB in *Pseudomonas aeruginosa*. *J Bacteriol* 193:2784–2792. <https://doi.org/10.1128/JB.00164-11>.
 41. O'Toole GA, Gibbs KA, Hager PW, Phibbs PV, Kolter R. 2000. The global carbon metabolism regulator Crc is a component of a signal transduction pathway required for biofilm development by *Pseudomonas aeruginosa*. *J Bacteriol* 182:425–431. <https://doi.org/10.1128/jb.182.2.425-431.2000>.
 42. Linares JF, Moreno R, Fajardo A, Mart nez-Solano L, Escalante R, Rojo F, Mart nez JL. 2010. The global regulator Crc modulates metabolism, susceptibility to antibiotics and virulence in *Pseudomonas aeruginosa*. *Environ Microbiol* 12:3196–3212. <https://doi.org/10.1111/j.1462-2920.2010.02292.x>.
 43. Andrade JM, Pobre V, Silva IJ, Domingues S, Arraiano CM. 2009. The role of 3'-5' exoribonucleases in RNA degradation. *Prog Mol Biol Transl Sci* 85:187–229. [https://doi.org/10.1016/S0079-6603\(08\)00805-2](https://doi.org/10.1016/S0079-6603(08)00805-2).
 44. Mass  E, Escorcia FE, Gottesman S. 2003. Coupled degradation of a small regulatory RNA and its mRNA targets in *Escherichia coli*. *Genes Dev* 17:2374–2383. <https://doi.org/10.1101/gad.1127103>.
 45. Allison KR, Brynildsen MP, Collins JJ. 2011. Metabolite-enabled eradication of bacterial persisters by aminoglycosides. *Nature* 473:216–220. <https://doi.org/10.1038/nature10069>.
 46. Peng B, Su YB, Li H, Han Y, Guo C, Tian YM, Peng XX. 2015. Exogenous alanine and/or glucose plus kanamycin kills antibiotic-resistant bacteria. *Cell Metab* 21:249–262. <https://doi.org/10.1016/j.cmet.2015.01.008>.
 47. Su YB, Peng B, Han Y, Li H, Peng XX. 2015. Fructose restores susceptibility of multidrug-resistant *Edwardsiella tarda* to kanamycin. *J Proteome Res* 14:1612–1620. <https://doi.org/10.1021/pr501285f>.
 48. Hoang TT, Karkhoff-Schweizer RR, Kutchna AJ, Schweizer HP. 1998. A broad-host-range Flp-FRT recombination system for site-specific excision of chromosomally-located DNA sequences: application for isolation of unmarked *Pseudomonas aeruginosa* mutants. *Gene* 212:77–86. [https://doi.org/10.1016/S0378-1119\(98\)00130-9](https://doi.org/10.1016/S0378-1119(98)00130-9).
 49. Choi KH, Schweizer HP. 2006. mini-Tn7 insertion in bacteria with single

- attTn7 sites: example *Pseudomonas aeruginosa*. Nat Protoc 1:153–161. <https://doi.org/10.1038/nprot.2006.24>.
50. Li M, Long Y, Liu Y, Liu Y, Chen R, Shi J, Zhang L, Jin Y, Yang L, Bai F, Jin S, Cheng Z, Wu W. 2016. HigB of *Pseudomonas aeruginosa* enhances killing of phagocytes by up-regulating the type III secretion system in ciprofloxacin induced persister cells. Front Cell Infect Microbiol 6:125. <https://doi.org/10.3389/fcimb.2016.00125>.
51. Loughman K, Hall J, Knowlton S, Sindeldecker D, Gilson T, Schmitt DM, Birch JW, Gajtka T, Kobe BN, Florjanczyk A, Ingram J, Bakshi CS, Horzempa J. 2016. Temperature-dependent gentamicin resistance of *Francisella tularensis* is mediated by uptake modulation. Front Microbiol 7:37. <https://doi.org/10.3389/fmicb.2016.00037>.
52. Weng Y, Chen F, Liu Y, Zhao Q, Chen R, Pan X, Liu C, Cheng Z, Jin S, Jin Y, Wu W. 2016. *Pseudomonas aeruginosa* enolase influences bacterial tolerance to oxidative stresses and virulence. Front Microbiol 7:1999. <https://doi.org/10.3389/fmicb.2016.01999>.
53. Sun Z, Shi J, Liu C, Jin Y, Li K, Chen R, Jin S, Wu W. 2014. PrtR homeostasis contributes to *Pseudomonas aeruginosa* pathogenesis and resistance against ciprofloxacin. Infect Immun 82:1638–1647. <https://doi.org/10.1128/IAI.01388-13>.